Density response in laterally modulated two-dimensional electron systems

P. W. Park,* A. H. MacDonald, and W. L. Schaich
Department of Physics, Indiana University, Bloomington, Indiana 47405
(Received 11 March 1992; revised manuscript received 24 July 1992)

We have evaluated within the random-phase approximation the density-response function of laterally modulated two-dimensional electron systems, examining both single-particle and collective behavior. By varying model parameters we can produce crossovers between different response characteristics. When the lateral period is long compared to the Fermi wavelength, the excitation spectrum evolves as the modulation strength is increased from a regime of plasmon bands with small gaps to a regime of geometrically confined plasmons. Simpler theories which ignore nonlocal effects in the response kernel can provide a qualitative picture of both these extremes but fail to describe the complicated crossover behavior between them. The simpler theories also fail completely when the lateral period becomes comparable to or smaller than the Fermi wavelength. Our fully quantum-mechanical evaluations show how in this limit the response behavior changes from that of Landau-broadened plasmons at weak modulation to that of depolarization-shifted intersubband transitions at strong modulation.

I. INTRODUCTION

There has been strong interest over recent years in the optical and transport properties of a two-dimensional electron gas in which motion in either one or both directions is altered by lateral modulation.[1] Theoretical work on the response properties of such laterally structured two-dimensional electron systems (LS2DEG) has mostly restricted its attention to particular limits where important simplifications are possible. Early work[2–9] focused on the bands of plasmonlike excitations that arise when the lateral structure has a period much greater than the 2D Fermi wavelength. The analysis was based on so-called semiclassical theories which approximate nonlocal effects in the response kernel but which were expected to be valid in the long-period limit. On the other hand, the objective of most experimental work has been to push toward the regime where quantum effects of the lateral structure become dominant and to identify features in experimental results which emerge as a consequence. In this regime the semiclassical approaches are not applicable and microscopic quantum calculations which properly treat nonlocal effects are required. Motivated by continuing experimental advances, recent theoretical studies[10–27] have discussed fully quantum-mechanical descriptions of LS2DEG but have usually (but not always, e.g., Ref. 17) assumed both that the modulation is strong and the period is short so only one or a few subbands are occupied. The response behavior is then dominated by distinct intersubband transitions within a single well. In this paper we report numerical work which extends the fully quantum-mechanical theory to the regime of most present experiments wherein the lateral period is still several times larger than the Fermi wavelength and many subbands are partially occupied.

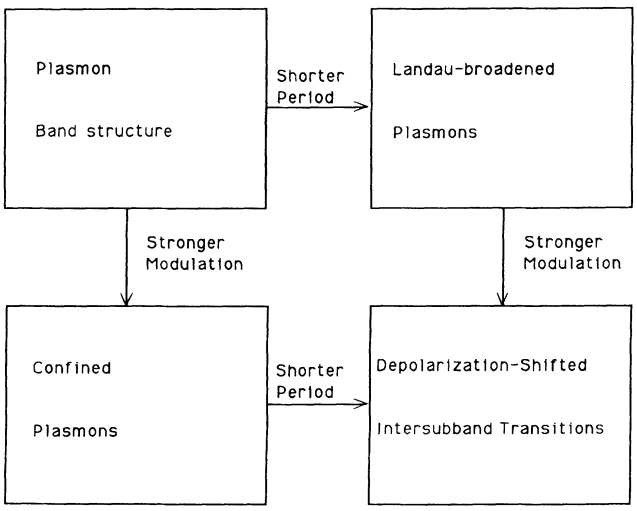

FIG. 1. Different regimes of response behavior in laterally structured two-dimensional electron systems.

It is useful to distinguish four different regimes in which the transport and optical properties of LS2DEG are qualitatively different. These are shown schematically in Fig. 1. Crossovers occur when the lateral period becomes shorter than the Fermi wavelength and/or when the modulation potential strength becomes larger than the Fermi energy. We will illustrate the changes which occur in the density response of the LS2DEG as these crossovers occur. By comparing the results of semiclassical and fully quantum-mechanical descriptions we are able to establish the regime of validity of the simpler theories used in earlier works. In Sec. II we briefly summarize our theory for the density-response functions of LS2DEG. Then in Sec. III we present results from several model calculations and discuss the trends and characteristic behaviors they illustrate.

II. RANDOM-PHASE APPROXIMATION

We begin with some formal but general expressions for a 2D system of total area A. In real space the density-

response function χ is defined by the first-order relation

$$\delta n(\mathbf{X},\omega)=\int d^2\mathbf{X}'\chi(\mathbf{X},\mathbf{X}';\omega)V_e(\mathbf{X}',\omega)\ , \tag{1}$$

where V_e is the external potential energy, δn is the induced density, ω is the driving frequency, and the vectors are two dimensional. For the random-phase approximation (RPA) one assumes the system responds like noninteracting electrons to the joint influence of the external potential plus the potential produced by the induced Hartree density:

$$\delta n(\mathbf{X},\omega)=\int d^2\mathbf{X}'\chi^0(\mathbf{X},\mathbf{X}';\omega)V_t(\mathbf{X}',\omega)\ , \tag{2}$$

where χ^0 is the susceptibility of independent electrons and the total potential energy $V_t=V_e+V_i$, with V_i the induced Hartree potential. Incorporating this into Eq. (2) we obtain an integral equation for χ, which in wave-vector space appears as

$$\chi(\mathbf{Q},\mathbf{Q}';\omega)=\chi^0(\mathbf{Q},\mathbf{Q}';\omega)+\sum_{\bar{\mathbf{Q}}}\chi^0(\mathbf{Q},\bar{\mathbf{Q}};\omega)v(\bar{\mathbf{Q}})\chi(\bar{\mathbf{Q}},\mathbf{Q}';\omega)\ , \tag{3}$$

where $v(\mathbf{Q})=2\pi e^2/Q\epsilon$, with ϵ the dielectric constant of the host in which the 2D system is immersed. Using Bloch states labeled by (reduced) wave vector $\mathbf{K}$ and band index n, we obtain for χ^0

$$\chi^0(\mathbf{Q},\mathbf{Q}';\omega)=\frac{2}{A}\sum_{\substack{n\mathbf{K}\\ n'\mathbf{K}'}}\frac{f_{n\mathbf{K}}-f_{n'\mathbf{K}'}}{\epsilon_{n\mathbf{K}}+\hbar\omega-\epsilon_{n'\mathbf{K}'}+i0^+}\times\langle n\mathbf{K}|\rho_{\mathbf{Q}}|n'\mathbf{K}'\rangle\langle n'\mathbf{K}'|\rho^\dagger_{\mathbf{Q}'}|n\mathbf{K}\rangle\ , \tag{4}$$

where the $f_{n\mathbf{K}}$ are Fermi-Dirac functions of the energy $\epsilon_{n\mathbf{K}}$ and the operators $\langle\mathbf{X}|\rho_{\mathbf{Q}}|\mathbf{X}'\rangle=e^{-i\mathbf{Q}\cdot\mathbf{X}}\delta(\mathbf{X}-\mathbf{X}')$ appear in the matrix elements.

Since we assume that there is no applied magnetic field, time reversal invariance holds. This implies that

$$\langle n\mathbf{K}|\rho_{\mathbf{Q}}|n'\mathbf{K}'\rangle=\langle n'-\mathbf{K}'|\rho_{\mathbf{Q}}|n-\mathbf{K}\rangle \tag{5}$$

and $\epsilon_{n\mathbf{K}}=\epsilon_{n-\mathbf{K}}$, which allows us to transform Eq. (4) into

$$\chi^0(\mathbf{Q},\mathbf{Q}';\omega)=\frac{2}{A}\sum_{\substack{n\mathbf{K}\\ n'\mathbf{K}'}}f_{n\mathbf{K}}\frac{2(\epsilon_{n\mathbf{K}}-\epsilon_{n'\mathbf{K}'})}{(\epsilon_{n\mathbf{K}}-\epsilon_{n'\mathbf{K}'})^2-\hbar^2\omega^2}\times\langle n\mathbf{K}|\rho_{\mathbf{Q}}|n'\mathbf{K}'\rangle\langle n'\mathbf{K}'|\rho^\dagger_{\mathbf{Q}'}|n\mathbf{K}\rangle\ . \tag{6}$$

In this form we see that for $\hbar\omega$ much larger than the significant particle-hole excitation energies,

$$\chi^0(\mathbf{Q},\mathbf{Q}';\omega)\to c(\mathbf{Q},\mathbf{Q}')/\omega^2\ , \tag{7}$$

with

$$c(\mathbf{Q},\mathbf{Q}')=\frac{-4}{\hbar^2 A}\sum_{n\mathbf{K}}f_{n\mathbf{K}}\langle n\mathbf{K}|H\rho_{\mathbf{Q}}\rho^\dagger_{\mathbf{Q}'}-\rho_{\mathbf{Q}}H\rho^\dagger_{\mathbf{Q}'}|n\mathbf{K}\rangle\ , \tag{8}$$

where $H|n\mathbf{K}\rangle=\epsilon_{n\mathbf{K}}|n\mathbf{K}\rangle$. Again using time-reversal symmetries, we can reexpress Eq. (8) as

$$c(\mathbf{Q},\mathbf{Q}')=\frac{2}{\hbar^2 A}\sum_{n\mathbf{K}}f_{n\mathbf{K}}\langle n\mathbf{K}|[\rho_{\mathbf{Q}},[H,\rho^\dagger_{\mathbf{Q}'}]]|n\mathbf{K}\rangle\ , \tag{9}$$

and working out the commutators we finally obtain

$$c(\mathbf{Q},\mathbf{Q}')=\frac{\mathbf{Q}\cdot\mathbf{Q}'}{m^*}N_0(\mathbf{Q}-\mathbf{Q}')/A\ , \tag{10}$$

where $N_0(\mathbf{Q})=\int d^2\mathbf{X}\,e^{-i\mathbf{Q}\cdot\mathbf{X}}N_0(\mathbf{X})$ is the Fourier transform of the equilibrium electron density and m^* is the (presumed isotropic) effective mass for the kinetic energy in H. Thus in the high-frequency limit

$$\chi^0(\mathbf{Q},\mathbf{Q}';\omega)\to\frac{\mathbf{Q}\cdot\mathbf{Q}'}{m^*\omega^2}\frac{N_0(\mathbf{Q}-\mathbf{Q}')}{A}\ . \tag{11}$$

The simple expression on the right-hand side of Eq. (11) is what most versions of the semiclassical theories use for χ^0 at all frequencies. Our derivation suggests that the collective modes predicted by such theories may only be accurate when their frequencies are well above those of the single-particle excitations from which they are constructed.

Now we specialize to the case where the LS2DEG is modulated in one direction only (the y direction), and use a Kronig-Penney (KP) potential to model the effective ground-state potential-energy profile seen by each electron. This parametrization scheme avoids the difficult experimental question of what confining potential need be applied. If we choose the origin for y to preserve inversion symmetry, then the χ^0 (and χ) functions obey $\chi^0(\mathbf{Q},\mathbf{Q}';\omega)=\chi^0(-\mathbf{Q},-\mathbf{Q}';\omega)$. We study the density response as the strength of the modulation potential (i.e., the height of the step barriers) is increased from zero to several times the Fermi energy at various modulation periods. The external perturbation is assumed to vary only in the same direction as the KP potential. This suppresses the appearance of some excitations,[23,28] but corresponds to the usual experimental configurations.[1] Notationally we replace

$$\mathbf{Q}\to\hat{y}Q^s=\hat{y}\left[q+\frac{2\pi s}{d}\right]\ , \tag{12}$$

where d is the KP period and $|q|<\pi/d$. Since the reduced wave vector q is "conserved" in the response functions, we write

$$\chi^0(\mathbf{Q},\mathbf{Q}';\omega)\to\chi^0_{s,s'}(q,\omega)\ , \tag{13}$$

with a similar replacement for χ. The basic RPA Eq. (3) then becomes the matrix equation

$$\chi_{s,s'}(q,\omega)=\chi^0_{s,s'}(q,\omega)+\sum_{\bar{s}}\chi^0_{s,\bar{s}}(q,\omega)v(Q^{\bar{s}})\chi_{\bar{s},s'}(q,\omega) \tag{14}$$

at fixed q and ω. We have solved Eq. (14) by truncating the plane-wave expansions at sufficiently large values of $|s|$. The accuracy of our calculations was confirmed[29] by separate checks on the two extreme limits of zero or infinite modulation strength. In the former case analytic

results for χ^0 are known,[30] while in the latter case of isolated quasi-one-dimensional systems the flat subbands also allow some parts of the calculation to be performed analytically.

III. MODEL CALCULATIONS

All the calculations we will discuss here were performed for LS2DEG at zero temperature with an average electron density $N_0(\mathbf{Q}=0)/A = N = 1.6\times10^{11}$ cm^{-2}, an effective mass $m^*/m = 0.066$, and a background dielectric constant $\epsilon = 12.7$. These parameter values are typical of LS2DEG constructed in GaAs. The effect of lateral structure on both χ^0 and χ will be exhibited by showing how the imaginary part of their diagonal matrix elements are changed. We use $q = 0$ in these calculations to be relevant to infrared-absorption experiments,[31] and plot versus energy scaled by

$$t \equiv \frac{\hbar^2\pi^2}{2m^*d^2} \simeq \frac{5700 \text{ meV}}{(d\ [nm])^2} . \tag{15}$$

The imaginary part of $\chi^0_{s,s}$ gives information about the excitation energies which would be important if the electrons did not interact. By examining the differences between the imaginary parts of $\chi^0_{s,s}$ and $\chi_{s,s}$ we can see directly the effect of electron-electron interactions on the excitation energies of a LS2DEG. These imaginary parts are conveniently extracted by letting $\omega \to \omega + i\gamma$ in appropriate places, where $\gamma = 0.5t$. The subtlety of this replacement in response functions was first discussed by Mermin[32] for homogeneous systems. We use the generalization of his prescription that was developed for inhomogeneous systems by Garik and Ashcroft.[33]

We first present a benchmark calculation,[30] showing in Fig. 2 the response of a uniform electron gas at integer multiples of $2\pi/d$ with $d = 150$ nm. For this "period"

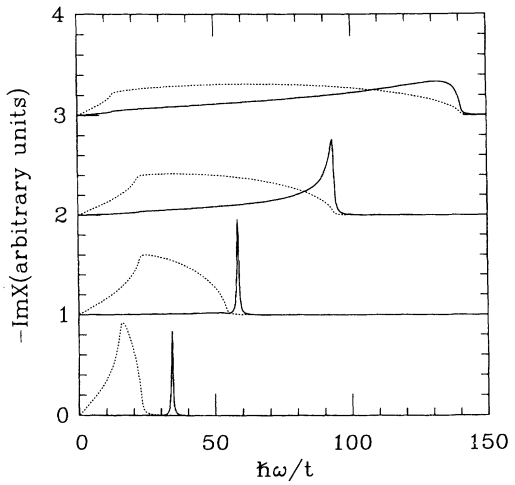

FIG. 2. Imaginary part of density-response functions of a uniform 2D electron gas vs driving frequency. The solid curves are Imχ and the dashed are Imχ^0. The probe wave vector $Q^s = s(2\pi/d)$ with $d = 150$ nm has $s = 1,2,3,4$ as one moves from the bottom to the top panel.

the energy unit is $t = 0.25$ meV and using $k_F^0 = (2\pi N)^{1/2}$ we find $k_F^0 d/\pi = 4.787$. Hence when the probe wave vector increases from $2\pi/d$ to $8\pi/d$ it grows from more than a factor of 2 below k_F^0 to almost a factor of 2 above k_F^0. In drawing the separate panels of the imaginary parts of $\chi^0_{s,s}$ and $\chi_{s,s}$ we have here (and in later figures) separately scaled their magnitudes so they fit within a unit vertical range. One can recreate their unscaled values by using the sum rule

$$-\int_0^\infty d\omega\, \omega\, \mathrm{Im}\chi^0(\mathbf{Q},\mathbf{Q}';\omega) = \frac{\pi}{2}\frac{\mathbf{Q}\cdot\mathbf{Q}'}{m^*}\frac{N_0(\mathbf{Q}-\mathbf{Q}')}{A} , \tag{16}$$

which follows from using the asymptotic form (11) in the Kramers-Kronig relations[34] for χ^0. Since the same formal limit also holds for χ, so does the sum rule (16).

There are significant changes in the density response for increasing Q^s in Fig. 2. The range of nonzero Im$\chi^0_{s,s}$ grows more rapidly than Q^s does, its upper edge overtaking the collective mode peak in Im$\chi_{s,s}$. Stated another way, the plasmon merges into the single-particle continuum for Q^s near k_F^0. In the lowest panel the plasmon peak in Imχ is still reasonably above the particle-hole continuum of Imχ^0, and the simplest semiclassical estimate of its position

$$\omega_s^2 = \frac{2\pi e^2 N Q^s}{\epsilon m^*} \tag{17}$$

yields $29.3t$ for $s = 1$, which is only 10% below the $s = 1$ peak in Fig. 2. For $s = 2$, Eq. (17) is about 30% too low, and for still higher s it becomes irrelevant because the results show that a sharp collective resonance has ceased to exist. A similar sort of failure of the semiclassical theory occurs often below.

We begin our numerical study of LS2DEG in the limit of long periods and weak modulation, where one expects the semiclassical approaches to be valid. We use a period of $d = 450$ nm made from a well width $a = 300$ nm and a step barrier width of $d - a$. The size of the energy unit is $t = 0.028$ meV and $k_F^0 d/\pi = 14.36$, so 15 subbands are partially occupied in the zero modulation limit. The large value of k_F^0 also implies that for $s \leq 4$, Q^s will remain well below k_F^0.

The first modulation potential that we illustrate for this period is $V/t = 50$. (V is the height of the KP step barriers above the energy zero at the bottom of the wells.) This value of V is weak since it is roughly four times smaller than the Fermi energy of the unmodulated system, which may be found from $E_F^0/t = (k_F^0 d/\pi^2)$. The KP bands are plotted in Fig. 3 and we label them here (and below) according to increasing energy starting with 1. Note that only the first few are significantly altered from free-electron behavior. Not surprisingly then, the continua of incoherent particle-hole contributions to χ^0 plotted in Fig. 4 are very similar to those for an unmodulated structure. The deviations, which are especially strong at low energies, arise from structure in the transition density of states. We also show in Fig. 4 the effect of interactions on the response of the system. There are

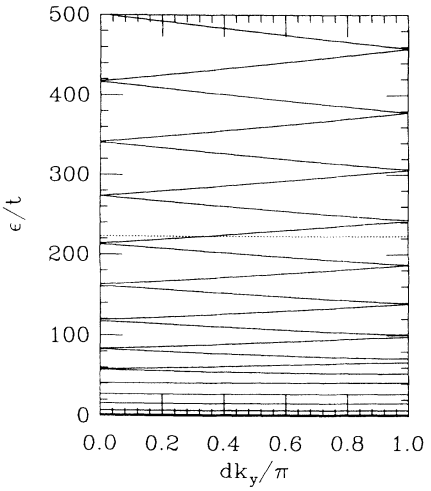

FIG. 3. Kronig-Penney bands for a model with $V/t=50$, $d=450$ nm, and $a=300$ nm. The Fermi level is at the dashed line.

sharp collective excitations at frequencies always located above the corresponding single-particle continuum. The plasmon energies are fairly well described by the semiclassical estimates, especially if one augments Eq. (17) with a $(\beta Q^s)^2$ term.[4] Semiclassical theory also successfully predicts the plasmon splitting that can be resolved in Fig. 4 for $s=1,2$. The relative size of the plasmon gap at Q^s should be set by the ratio $|N_0(4\pi s/d)|/N_0(0)$.[2,3] In Table I we compare this ratio with $\Delta\omega/\bar{\omega}$, where for each resolvable pair of peak locations, $\omega_\pm$, we define $\Delta\omega=\omega_+-\omega_-$ and $\bar{\omega}=(\omega_++\omega_-)/2$.

We have confirmed by our fully quantum-mechanical theory that semiclassical predictions are fairly reliable in

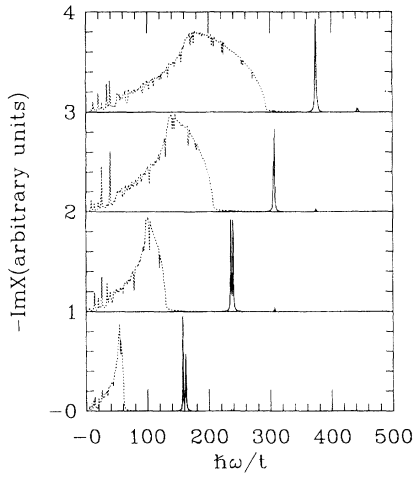

FIG. 4. Imaginary part of the diagonal density-response matrices for a LS2DEG, $\chi^0_{s,s}(q,\omega)$ and $\chi_{s,s}(q,\omega)$, vs frequency. Here $q=0$ and s increases from 1 to 4 as one moves up through the panels. Within each panel the plotted functions have been separately scaled to fit. The dashed curves are for χ^0 and the solid for χ. The Kronig-Penney parameters are those of Fig. 3.

TABLE I. Comparison of relative plasmon gap with semiclassical theory.

s	$\hbar\omega_-/t$	$\hbar\omega_+/t$	$\Delta\omega/\bar{\omega}$	$\lvert N_0(4\pi s/d)\rvert/N_0(0)$
1	157.5	162.0	0.028	0.034
2	235.5	239.0	0.015	0.016

the upper left part of Fig. 1. Now we want to illustrate how moving away from this limit leads to both quantitative and qualitative failures. One might think that the easiest extension for the semiclassical theories would be to increase the modulation strength at long periods. Then the basic collective modes remain the plasmons, with only their dispersion being modified. Qualitatively this is true, but quantitative accuracy is lost. Let us jump to the limit of strong modulation using $V/t=500$. The Fermi energy at this modulation strength allows for the partial occupation of the first 12 KP subbands shown in Fig. 5. Many of the lower KP bands are flat and the incoherent excitations between them are strongly peaked near mean intersubband transition energies, which themselves approach the transition energies of an isolated well. To quantify these claims about the bands, note that $\epsilon_{n\mathbf{K}}/t=\epsilon_{nk_y}/t+(dk_z)^2$. For flat bands $\epsilon_{nk_y}\to\epsilon_n$ and we consider whether

$$\epsilon_n/t=\left[\frac{d}{a^*}n\right]^2. \tag{18}$$

For the bands in Fig. 5, we find that Eq. (18) describes the first 15 bands to better than 5% with the choice $a^*/a=1.043$. The higher bands quickly deviate from Eq. (18) and develop dispersion when their energy rises above V.

From Fig. 6 we can identify 12 sharp peaks corresponding to transitions from each of the occupied bands to the next higher band, 12 peaks corresponding to band

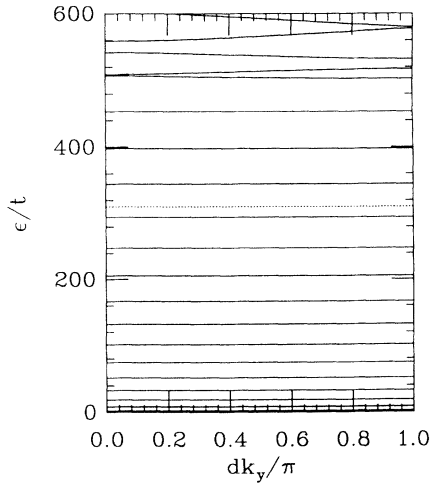

FIG. 5. Kronig-Penney bands for a model with $V/t=500$, $d=450$ nm, and $a=300$ nm. The Fermi level is at the dashed line.

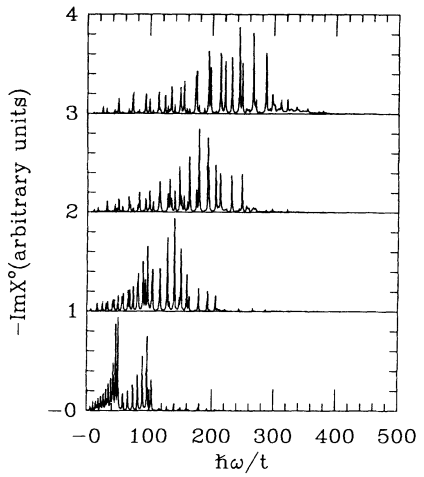

FIG. 6. Imaginary part of the diagonal density-response matrix for independent electrons, $\chi^0_{s,s}(q,\omega)$ vs frequency. The plotting scheme is the same as in Fig. 4, while the Kronig-Penney parameters are those of Fig. 5.

index changes of two and so on. Bandlike features begin to develop for band index changes of four or more as transitions to dispersive, higher-energy KP bands become possible. The peaks with larger band index changes are, of course, at higher energies and have larger weight in the higher wave-vector diagonal matrix elements. Since the bound states within a well must have an integral number of half-wavelengths there, the low-lying interband transitions where the band index changes by j correspond to a wave-vector change[35] of $j\pi/a$ and in the limit of wide quantum wells their contribution is like that of a uniform system at this wave vector. This idea is confirmed in Fig. 6 by the fact that the envelope of contributions from a band index change of one is similar in shape to the corresponding free-electron curve.

The effect of interactions is shown in Fig. 7. The qualitative change in the response of the system from Fig. 6 is analogous to that between the curves in Fig. 4. A few sharp modes appear in place of the many intersubband transitions. These modes are exactly the confined plasmon excitations which have long[4−8] been anticipated theoretically on the basis of semiclassical theories and have recently[36,37] been seen experimentally. The modes are expected to occur in the simplest approximation[38] at the frequencies[4−8]

$$\omega_C^2 = 2\pi^2 N_w e^2 k/\epsilon m^* a \ , \tag{19}$$

where k is an integer and N_w is the electron density in the well. The lowest five resonance energies predicted by Eq. (19) using $N_w = dN/a$ for the situation of Fig. 7 are in units of t 162, 229, 280, 323, and 361, which do not agree with the RPA peak positions except (accidently) for the second lowest mode. We have checked by further calculations under strong confinement conditions that the dependence of the lowest RPA mode on the well width and density is, however, qualitatively the same as suggested by Eq. (19). At the next level of semiclassical approximation one can solve Eq. (3) for a single well with infinite confining barriers using Eq. (11) for χ^0 with a constant equilibrium density $N_0(\mathbf{X}) \approx N_w$ within the well. We then find[39] for the lowest five confined plasmons 139, 214, 268, 313, and 352 in units of t. This set agrees better with our results. We also tried to further improve the semiclassical predictions by using the calculated ground-state density for the whole superlattice in Eq. (11). However, we found that this more sophisticated evaluation[4−9] gives worse quantitative estimates.[29] We obtained for the specific case of Fig. 7 6, 19, 75, 112, 197, 211, 274, and 298 in units of t for the eight lowest modes. The spurious appearance of low-frequency modes when $N_0(\mathbf{X})$ smoothly varies down to small values is a general defect of semiclassical estimates.[29]

Matters are even worse for the semiclassical theories at intermediate modulation strengths. For instance, we evaluated χ^0 and χ when $V/t = 300$ and 13 KP subbands are partially occupied.[29] The spectrum of Imχ^0 then has sharp δ-function-like contributions riding on a smooth background. The former are due to transitions among the lowest ten bands which are nearly dispersionless, while the latter arises from transitions among the higher bands. However, unlike the cases of either weak or strong modulation in Figs. 4 and 7, the spectrum of Imχ is bandlike rather than δ-function-like. There are no sharp collective resonances of the system at this modulation strength, so the semiclassical theories (which predict plasmon modes at every modulation strength) fail qualitatively.

The semiclassical theories also fail when one moves to the right-hand side of Fig. 1. Considering first that the modulation is weak, moving to the upper right of Fig. 1 means examining the plasmon modes at increasing wave vectors where they interact more strongly with the particle-hole continuum, physics that is illustrated in Fig. 2 but ignored by the semiclassical theories. To move far into this regime we consider results for a KP potential with $d = 50$ nm and $a = 20$ nm. These widths are shorter

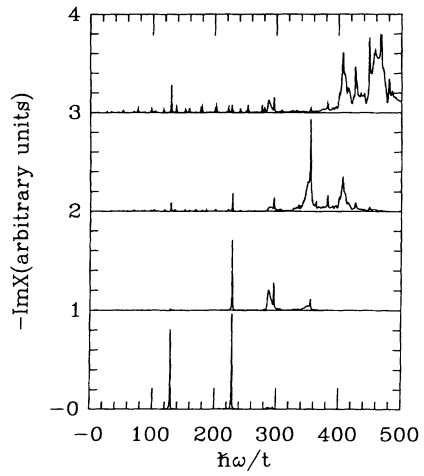

FIG. 7. Imaginary part of the diagonal density-response matrix for interacting electrons, $\chi_{s,s}(q,\omega)$, vs frequency. The plotting scheme is the same as in Fig. 4, while the Kronig-Penney parameters are those of Fig. 5.

than what is achievable with present-day microstructuring technology. At this period our energy unit is $t=2.3$ meV and $k_F^0 d/\pi=1.596$, so there will be two occupied subbands in the limit of zero modulation strength. Since the first nonzero wave vector we probe in the LS2DEG is $2\pi/d$, even it is larger than k_F^0, and hence, recalling the upper panels of Fig. 2, one should not expect true plasmon excitations in this system.

The weakest modulation potential that we illustrate for this period is $V/t=4$, whose KP bands are shown in Fig. 8. The continuum of incoherent excitations shown in Fig. 9 is strongly distorted but still recognizably similar to the corresponding unmodulated results. The various dips are due to the small gaps between the higher bands. The influence of interactions is also shown in Fig. 9. It appears that they merely shift the bands of incoherent excitation toward higher frequencies, without producing any sharp collective excitations. The same qualitative behavior occurs in Fig. 2.

The pictures change if we move to strong modulation; i.e., into the lower right of Fig. 1. We show in Fig. 10 the KP bands for the choice $V/t=200$, which is more than an order of magnitude greater than E_F^0/t. The parametrization of Eq. (18) is accurate here to within 5% for the first five bands with the choice $a^*/a=1.113$. Unlike the case for $V/t=4$, only the lowest subband is occupied. Over the frequency range shown in Fig. 11, we see sharp, separable contributions to χ^0 coming from transitions between the first band and the second, third, and fourth bands. The peak locations are consistent with Eq. (18); i.e., with the energy separations of the eigenstates of an isolated square well. When we compare χ^0 and χ in Fig. 11, we notice that the effect of interactions is merely to shift these excitation peaks up by about four, three, and two energy units for the $1\rightarrow2$, $1\rightarrow3$, and $1\rightarrow4$ transitions, respectively. These shifts are the depolarization shifts of the intersubband transitions that determine χ^0.

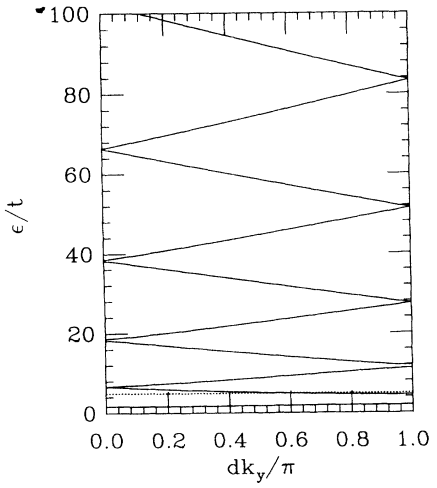

FIG. 8. Kronig-Penney bands for a model with $V/t=4$, $d=50$ nm, and $a=20$ nm. The Fermi level is at the dashed line.

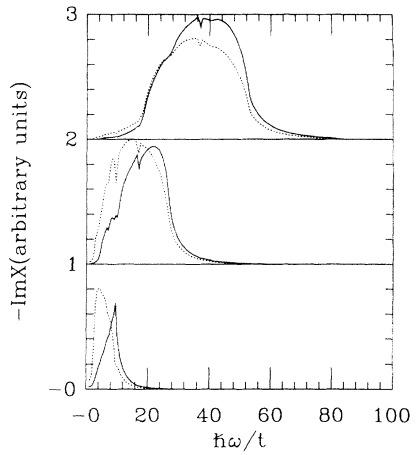

FIG. 9. Imaginary part of the diagonal density-response matrices for a LS2DEG, $\chi^0_{s,s}(q,\omega)$ and $\chi_{s,s}(q,\omega)$, vs frequency. The plotting scheme is the same as in Fig. 4, while the Kronig-Penney parameters are those of Fig. 8.

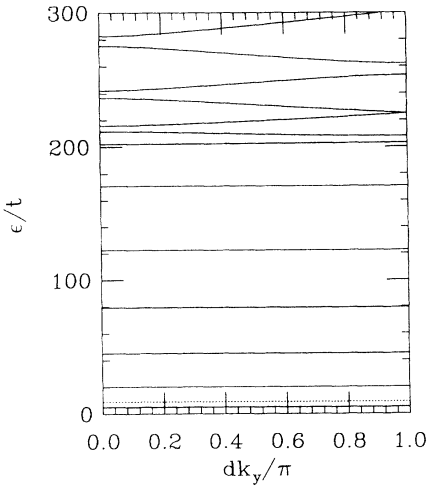

FIG. 10. Kronig-Penney bands for a model with $V/t=200$, $d=50$ nm, and $a=20$ nm. The Fermi level is at the dashed line.

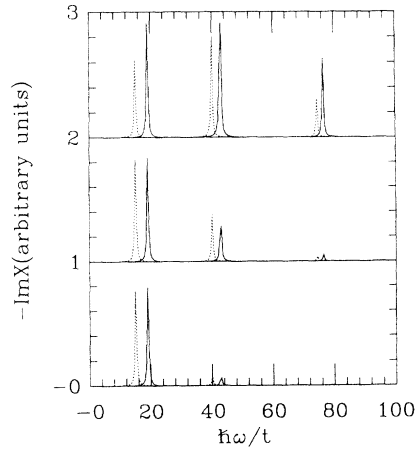

FIG. 11. Imaginary part of the diagonal density-response matrices for a LS2DEG, $\chi^0_{s,s}(q,\omega)$ and $\chi_{s,s}(q,\omega)$, vs frequency. The plotting scheme is the same as in Fig. 4, while the Kronig-Penney parameters are those of Fig. 10.

The limit of isolated wells has been discussed by earlier workers,[10,12,14,15,18–20] and their results may be formally recovered from the flat-subband limit of our theory. The depolarization shifts are expected to be of order[12,15]

$$\Delta \approx e^2 dN/\epsilon = 0.18 \text{ meV} d \text{ [nm]} = 9 \text{ meV} , \quad (20)$$

with dN acting as the linear density of an isolated channel. This estimate is consistent with the size of the shifts between the peaks in Fig. 11.

When the depolarization shifts are small compared to the intersubband transition energies, each excitation energy of the interacting system may be associated with a definite transition. When the depolarization shifts become comparable to the differences between the intersubband energies, the various excitations which exist in the noninteracting system are strongly coupled together by interactions and it is no longer easy to associate the peaks in χ with particular intersubband transitions. For the case where only a few subbands are occupied, the intersubband transition energies are, at strong modulation, of the order of our energy unit while the characteristic energy scale for interactions is set by the Δ of Eq. (20). The importance of interactions in coupling intersubband transitions is determined then (for our fixed N) by the ratio

$$\frac{\Delta}{t} \approx 3.2 \times 10^{-5} (d \text{ [nm]})^3 . \quad (21)$$

One should therefore expect intersubband excitations to be strongly mixed by interactions only for d greater than 100 nm in our systems. This is consistent with our finding that the intersubband excitations are not strongly mixed by interactions for $d = 50$ nm, but are so mixed for the larger d considered below. As an aside we caution that the crossover value of d depends on the choice of N. Li and Das Sarma[18] produce in their model with a well width ~ 500 nm a picture of greatly shifted, but not strongly mixed, intersubband transitions. This occurs because they choose, in order to assure occupancy of just the lowest subband, a value for N more than two orders of magnitude smaller than ours.

We have so far only shown results from well inside the different regimes noted in Fig. 1. Now consider the choice of $d = 150$ nm, which puts us near the vertical boundary through the center of Fig. 1. One then has $E_F^0/t = 22.9$, so the values $V/t = 10$, 50, and 250 should put us in weak, intermediate, and strong modulation regimes, respectively. In Fig. 12 we show results for both $\text{Im}\chi^0_{1,1}$ and $\text{Im}\chi_{1,1}$ for each of these three cases.

For weak modulation we see a broad plasmon peak in $\text{Im}\chi$. The fine structure on its side is better interpreted as a remnant of the single-particle peaks in $\text{Im}\chi^0$ than as a split-plasmon resonance. In the middle panel of Fig. 12 we have a messy broadband spectrum for both $\text{Im}\chi^0$ and $\text{Im}\chi$. Such spectra are typical of the response at intermediate modulation strength.[17,29]

For strong modulation, one again has sharp peaks but their interpretation in $\text{Im}\chi$ is unclear. The peaks in $\text{Im}\chi^0$ are directly related to intersubband transitions. There are three occupied subbands and, e.g., the first three peaks in $\text{Im}\chi^0$ are at the energies of the $1 \rightarrow 2$, $2 \rightarrow 3$, and $3 \rightarrow 4$ transitions. The question is what happens to these peaks when interactions are included. The answer depends on one's point of view. Within the scenario of the lower right of Fig. 1, one can argue that the peak due to the $3 \rightarrow 4$ transition has acquired most of the others' oscillator strength and appears in $\text{Im}\chi$ with a strong depolarization shift at $55.5t$. Alternatively, with the view from the lower left of Fig. 1, one can claim that the peaks at $55.5t$ and $100t$ are simply the two lowest confined plasmons. We favor the first interpretation over the second since it gives one a picture of how the spectra evolve as the interactions turn on. This is illustrated in Fig. 13, where we treat the background dielectric con-

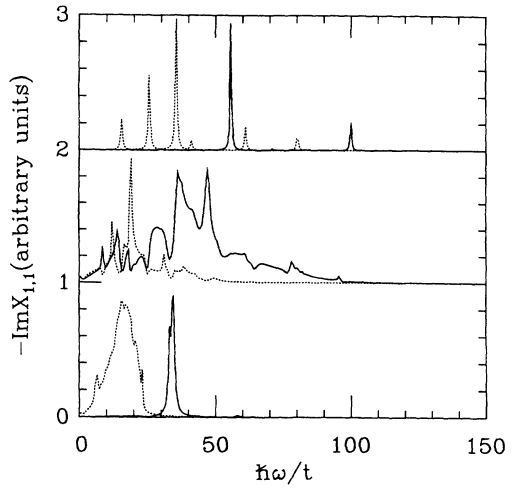

FIG. 12. Imaginary part of $\chi^0_{s,s}$ and $\chi_{s,s}$ for $s = 1$, $d = 150$ nm, and $a = 60$ nm vs frequency. The solid curves are $\text{Im}\chi$ and the dashed are $\text{Im}\chi^0$. The modulation strength increases through $V/t = 10, 50, 250$ as one moves from the bottom panel to the top.

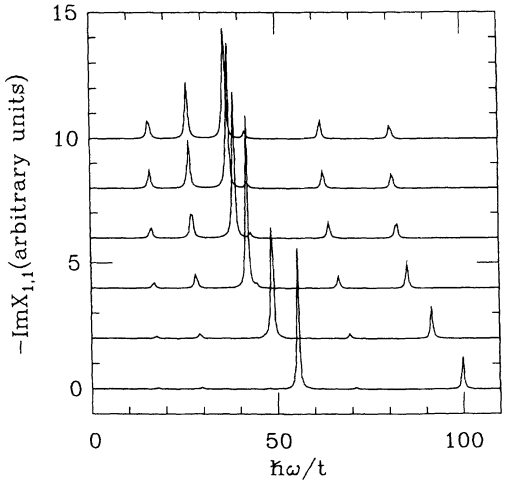

FIG. 13. Imaginary part of $\chi_{1,1}$ for $d = 150$ nm, $a = 60$ nm, $V/t = 250$, and variable ϵ vs frequency. As one moves from the top to the bottom of the plot, ϵ has the values 320, 160, 80, 40, 20, 12.7 and the results are vertically offset but scaled the same way.

stant as a free parameter in the calculation of χ from χ^0 via Eq. (14). Consider first the three lowest peaks. As the electron-electron coupling is increased (by decreasing ϵ), oscillator strength from the bottom two is smoothly transferred to the top one, until it alone is visible at a strongly shifted position. The same qualitative behavior occurs for the three highest peaks in $-\mathrm{Im}\chi^0$. For this trio the strongest peak in the absence of electron-electron interactions is the middle one (near $62t$), but it, along with the bottom one, eventually loses all of its oscillator strength to the top peak. We found similar evolution patterns for other choices of lateral period at strong modulation strength. Thus, although we have spoken of strong interactions "mixing" intersubband peaks, it is more appropriate to say that excitation strength is transferred among depolarization-shifted peaks rather than that peaks coalesce.

To summarize our results let us return to Fig. 1. Our evaluations have been carried out in and between all four regimes shown there and we found the different characteristic behaviors noted. We claim that only a fully quantum-mechanical theory is capable of quantitatively describing each regime and the complicated crossovers between them. Ours is certainly not the most sophisticated quantum-mechanical theory one could imagine for this task, but it has allowed us to carry through an initial numerical survey. In future work one might attempt to calculate the self-consistent ground-state potential-energy profile from an *a priori* confining potential, include estimates of exchange and correlation energies, and determine quantities that may be directly compared with experimental data.[31] These and other omitted effects will certainly change the quantitative results, but should not modify the qualitative classifications in Fig. 1.

ACKNOWLEDGMENTS

We thank Ulrich Wulf for a careful reading of the manuscript. This work was supported in part by the National Science Foundation through Grant Nos. DMR89-03851 and DMR91-13911. Some of the calculations were done on the Cray Research, Inc., Y-MP4/464 system at the National Center for Supercomputing Applications at the University of Illinois at Urbana–Champaign (Champaign, IL) under Grant No. DMR91-00014N.

*Present address: Basic Research Department, Electronics Technology Research Institute, Seoul, Korea.

[1]For recent reviews, see D. Heitmann, in *Quantum Coherence in Mesoscopic Systems,* edited by Bernhard Kramer (Plenum, New York, 1991); J. Kotthaus, in *Interfaces, Quantum Wells, and Superlattices,* edited by C. R. Leavens and Roger Taylor (Plenum, New York, 1988).

[2]M. V. Krasheninnikov and A. V. Chaplik, Fiz. Tekh. Poluprovodn. **15**, 32 (1981) [Sov. Phys. Semicond. **15**, 19 (1981)].

[3]A. V. Chaplik, Surf. Sci. Rep. **5**, 289 (1985).

[4]W. Y. Lai, A. Kobayashi, and S. Das Sarma, Phys. Rev. B **34**, 7380 (1986).

[5]G. Eliasson, J. W. Wu, P. Hawrylak, and J. J. Quinn, Solid State Commun. **60**, 41 (1986).

[6]G. Eliasson, P. Hawrylak, J. W. Wu, and J. J. Quinn, Solid State Commun. **60**, 3 (1986).

[7]V. Cataudella and G. Iadonisi, Phys. Rev. B **35**, 7443 (1987).

[8]G. Eliasson, P. Hawrylak, and J. J. Quinn, Phys. Rev. B **36**, 7631 (1987).

[9]V. Cataudella and V. M. Ramaglia, Phys. Rev. B **38**, 1828 (1988).

[10]A. V. Chaplik, Superlatt. Microstruct. **6**, 329 (1989).

[11]S. Das Sarma and W. Lai, Phys. Rev. B **32**, 1401 (1985).

[12]W. Que and G. Kirczenow, Phys. Rev. B **37**, 7153 (1988).

[13]V. Cataudella, Phys. Rev. B **38**, 7828 (1988).

[14]W. Que and G. Kirczenow, Phys. Rev. B **39**, 5998 (1989).

[15]Q. Li and S. Das Sarma, Phys. Rev. B **40**, 5860 (1989).

[16]D. Huang and S. Zhou, Phys. Rev. B **41**, 3847 (1990).

[17]C. Dahl, Phys. Rev. B **41**, 5763 (1990).

[18]Q. Li and S. Das Sarma, Phys. Rev. B **41**, 10 268 (1990).

[19]G. Y. Hu and R. F. O'Connell, Phys. Rev. B **42**, 1290 (1990); **44**, 3140 (1991).

[20]H. Yu and J. C. Hermanson, Phys. Rev. B **42**, 1496 (1990).

[21]U. Wulf, E. Zeeb, P. Gies, R. R. Gerhardts, and W. Hanke, Phys. Rev. B **42**, 7637 (1990).

[22]B. S. Mendoza and W. L. Schaich, Phys. Rev. B **43**, 6590 (1991).

[23]B. S. Mendoza and W. L. Schaich, Phys. Rev. B **43**, 9275 (1991).

[24]Q. P. Li and S. Das Sarma, Phys. Rev. B **43**, 11 768 (1991).

[25]L. Wendler, R. Haupt, and R. Pechstedt, Phys. Rev. B **43**, 14 669 (1991).

[26]G. Gumbs, D. Huang, and D. Heitmann, Phys. Rev. B **44**, 8084 (1991).

[27]R. Haupt, L. Wendler, and R. Pechstedt, Phys. Rev. B **44**, 13 635 (1991).

[28]B. S. Mendoza and W. L. Schaich (unpublished).

[29]P. W. Park, Ph.D. thesis, Indiana University, 1990.

[30]F. Stern, Phys. Rev. Lett. **18**, 546 (1967).

[31]The specific calculation of infrared transmission through a LS2DEG with a grating coupler is presented in the following paper [Phys. Rev. B **46**, 12 643 (1992)].

[32]N. D. Mermin, Phys. Rev. B **1**, 2362 (1970).

[33]P. Garik and N. W. Ashcroft, Phys. Rev. B **21**, 391 (1980).

[34]J. D. Jackson, *Classical Electrodynamics* (Wiley, New York, 1975).

[35]The eigenstates of an isolated well are standing waves. There is hence also a contribution to the matrix element which corresponds to the wave-vector change of $2n+j$ for transitions between bands n and $n+j$.

[36]T. Demel, D. Heitmann, P. Grambow, and K. Ploog, Phys. Rev. B **38**, 12 732 (1988).

[37]J. Alsmeier, E. Batke, and J. P. Kotthaus, Phys. Rev. B **40**, 12 574 (1989).

[38]It is not possible to derive an exact analytic expression for the resonance frequencies even in the semiclassical approximation.

[39]W. L. Schaich and A. H. MacDonald, Solid State Commun. (to be published).